

Article

Heterogeneities in the Cohesion of the Deposits of the 2021 Tajogaite Eruption of La Palma (Canary Islands, Spain)

Alfonso Ontiveros-Ortega ^{1,2}, José A. Moleón-Baca ¹, Raúl Huertas Mesa ¹, Isabel Abad ³
and Mario Sánchez-Gómez ^{3,*}

¹ Department of Physics, Campus Universitario Las Lagunillas s/n, University of Jaén, 23071 Jaén, Spain; aontiver@ujaen.es (A.O.-O.); jamoleon@ujaen.es (J.A.M.-B.); rhm00015@red.ujaen.es (R.H.M.)

² Instituto Andaluz de Geofísica, University of Granada, 18071 Granada, Spain

³ Department of Geology, Centro de Estudios Avanzados en Ciencias de la Tierra y el Medio Ambiente (CEACTEMA), Campus Universitario Las Lagunillas s/n, University of Jaén, 23071 Jaén, Spain; miabad@ujaen.es

* Correspondence: msgomez@ujaen.es; Tel.: +34-953-212775

Abstract: The present study analyzes the electrical and thermodynamic properties of the volcanic ash deposits from the recent eruption that started on 19 September 2021 in the Cumbre Vieja area on the island of La Palma. This work compares the analysis of the zeta potential and the surface free energy components of representative samples of unaltered tephra deposits with samples affected by the fumarolic activity near the emission zone, where sulfurous vapors were present. The results show that fumarolic activity modifies both the zeta potential and the surface free energy components of volcanic ash, decreasing its surface electrical charge and conferring less hydrophilicity on the deposit. Based on this, the interaction energies between ash particles in an aqueous medium have been calculated, in order to analyze the cohesion of the deposit and, where appropriate, its rheological properties, ending with the analysis of the effect produced by different chemical species on the surface charge and free energy of the ashes, and their influence on the cohesion of the deposit. The results confirm an attractive interaction energy between the ash particles and therefore greater stability to the deposit affected by fumarolic activity.

Keywords: tephra; surface free energy; zeta potential; cohesion; slope stability



Citation: Ontiveros-Ortega, A.; Moleón-Baca, J.A.; Mesa, R.H.; Abad, I.; Sánchez-Gómez, M.

Heterogeneities in the Cohesion of the Deposits of the 2021 Tajogaite Eruption of La Palma (Canary Islands, Spain). *Geosciences* **2023**, *13*, 346. <https://doi.org/10.3390/geosciences13110346>

Academic Editors: Jesus Martinez-Frias and Gianluca Groppelli

Received: 4 October 2023

Revised: 31 October 2023

Accepted: 8 November 2023

Published: 11 November 2023



Copyright: © 2023 by the authors. Licensee MDPI, Basel, Switzerland. This article is an open access article distributed under the terms and conditions of the Creative Commons Attribution (CC BY) license (<https://creativecommons.org/licenses/by/4.0/>).

1. Introduction

The stability of volcanic edifices is compromised over time with the changes that occur with respect to the initial conditions of the deposits [1]. These initial conditions depend largely on the type of eruption and on its geochemical nature. Knowledge of the initial conditions in the formation of the volcanic edifice is essential for the sequential monitoring of its geotechnical state and for the understanding of the mechanisms that justify its stability evolution.

The case of the Tajogaite eruption of Cumbre Vieja (La Palma, Canary Islands, September–December 2021) has had extensive and continuous monitoring of all the parameters that accompany the eruptive process since its inception. A continuous analysis of the seismicity, the deformation, the gas emission, the morphology of the erupted material, as well as its mineralogy and chemical composition, has been carried out [2,3]. In particular, the characteristics of the tephra deposits and their evolution over time have been analyzed [4,5].

In recent years, other lines of work have been added to the study of the dynamics of the volcanic edifice, based on the analysis of the physicochemical properties of the eruption materials, especially the more geotechnically unstable tephra deposits [6–8]. The superficial physicochemical properties of the samples allow us, among other things, to determine the states of aggregation and, therefore, to know the microstructure of these deposits, their

water-retention capacity, as well as their cohesion and rheological properties if flows as landslides or lahars [7–22].

The implications that the results of physical–chemical study have on the stability of the volcanic edifice are especially interesting [6,8,9,20,21,23]. The lack of stability is usually attributed to two processes, i.e., gravitational spreading and the inflation of a magma chamber within the volcano [24,25].

The deformations in the volcanic edifice are not distributed homogeneously, causing the morphology of the volcano to be varied. There is much evidence of landslides suffered by large stratovolcanoes, such as Etna [26], or volcanic edifices, such as El Hierro [6], Tenerife [8], or in Colima, Mexico [27]. These landslides are commonly produced using, as a slide plane, volcanic-ash deposits that have undergone hydration, weathering, and metal input by fumarolic activity or climate framework, which produce changes in the physical and chemical properties of the material [19,20,28].

The state of these deposits depends largely on the weather conditions; therefore, there will be different deposits from the same tephra type if it is subjected to different environmental conditions. It would be important to know the physical–chemical characteristics of the ashes from these deposits and their evolution with environmental parameters such as pH, chemical species present in the medium, and their concentration. In all these studies, there is a determining factor, poorly investigated, which is the modification experienced by the cohesion of the soil in the aging process of the deposits, due to the contribution of heavy metal salts from new eruptions [29], or from its release during the weathering process of the parent material [30,31].

In this work, a physical–chemical, mineralogical, and morphological characterization of ashes from a few stages of the Tajogaite eruption has been carried out. We have analyzed the surface physical–chemical properties of distinct ash samples: some affected by fumarolic activity and others unaltered from the early and late stages of the eruption. Based on this characterization, the cohesion of the deposit has been estimated by calculating the interaction energy between the ash particles that make it up. Moreover, we tested the effects of cation electrolytes at different concentrations and pH on the interaction energies between particles to simulate possible environmental scenarios that could alter the initial properties of the tephra.

The interactions between the smallest particles that constitute a soil are included in the extended DLVO theory (Derjaguin, Landau, Verwey and Overbeek), which also considers the acid–base structural interactions [32]. The quantification of these interactions requires an electrical and thermodynamic characterization of the material involved. The electrical characterization is carried out with the surface electrical charge determined from electrophoretic mobility measurements [33] and thermodynamics with the surface free energy obtained using the thin layer Wicking technique [34–36].

2. Materials and Methods

A first sampling was carried out on 27 September 2021, shortly after the onset of the eruption, at the Jable Astronomical observatory viewpoint (sample Jable-A, Figure 1), 1.7 km east of the pyroclastic vents, corresponding approximately to the first third of the so-called lower tephra unit [4]. The second survey was completed on 17 March 2022, three months after the end of the eruption, avoiding places where it could have started any incipient weathering process, but ensuring a sufficient period of time for the fumarolic activity to be effective on the tephra [37]. The field survey showed that the ash distribution around the volcano was homogeneous throughout the affected area, which has been confirmed by later work [4,5]. Three additional samples were collected (Figure 1): one in the proximity of the Jable-A sample, but in the upper tephra unit (Jable), to characterize unaltered ash, and the others around the craters located more to the southeast, where intense and extensive fumarolic activity has been described [38].

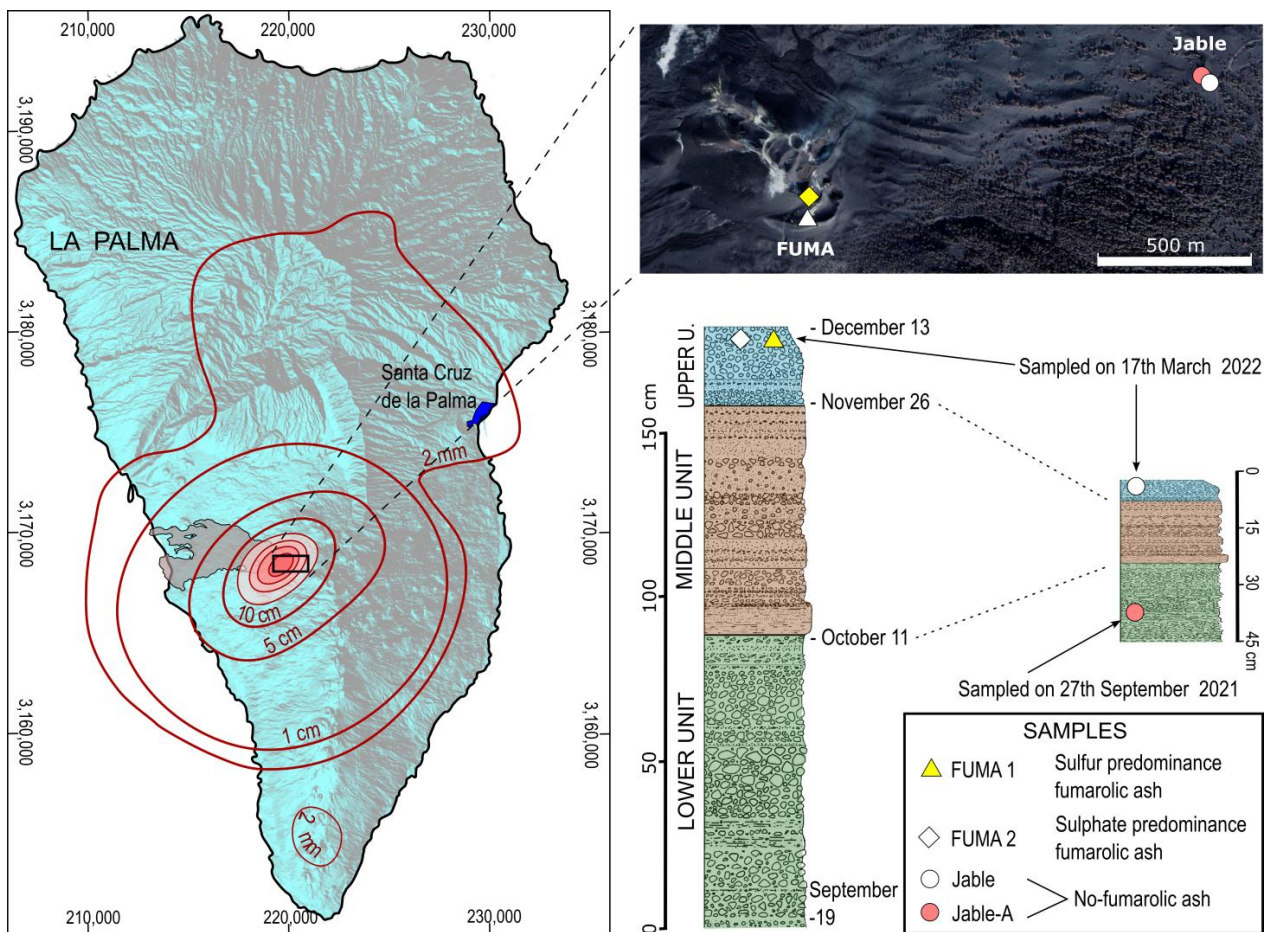


Figure 1. Tephra thickness distribution of the 2021 Tajogaite eruption. The white and yellow areas of the orthoimage represent fumarolic deposits with a predominance of sulphates and sulfur respectively, except in the NW corner which represents a cloud. The La Palma hillshade map is obtained from IGN MDT 25 m (WGS84, UTM Zone 28 N). The isolines depict isopachs of total tephra deposits (after [4] and IGME-CSIC map 28 September 2021). The shaded inner isopachs indicate successively thicknesses of 20, 50, 100, and 200 cm. The lava flow is drawn from COPERNICUS (2021). The orthoimage is from Google Earth (13 January 2022). The large tephra stratigraphic column (**left**) represents a reference point located 1 km SW from the tephra vents where three different volcano-sedimentary units have been identified (redrawn from [4,5]); the shorter stratigraphic column (**right**) was obtained in this work.

Fumarolically modified tephra outcrops in patches where sulfur and sulphate minerals are predominant [37]. Thus, samples FUMA 1 and FUMA 2 (Figure 1) correspond respectively to areas with a predominance of sulfur and sulphates that can be distinguished in outcrop by the intense yellow color of the sulfur.

The protocol for sampling was the following: the samples were superficial and corresponded to a square area with a side of 40 cm and a thickness between 1 and 2 cm; these were homogeneous in terms of grain size and color; samples were stored in a zip-lock bag and properly labeled.

2.1. Compositional and Textural Characterization

Tephra sample compositions were analyzed by wavelength dispersive X-ray fluorescence (XRF) using an S4 Pioneer Prior XRF (Centro de Instrumentación Científico-Técnica, CICT, Universidad de Jaén, Jaén, Spain). Samples were crushed to ensure a uniform texture and particle-size distribution, and then pressed into tablet form using a hydraulic press (model MIGNON SS, Nannetti, Faenza, Italy). All reagents and chemicals were of analytical

grade (Merck KGaA and Sigma-Aldrich Co. LLC, Darmstadt, Germany). The quantitative analysis of the material was done via X-ray fluorescence (XRF) spectrometry.

For mineralogical characterization, X-ray diffraction (XRD) patterns of samples were obtained from powders with an Empyrean diffractometer (PANalytical) equipped with a θ/θ goniometer (CICT, Universidad de Jaén, Jaén, Spain). The $\text{CuK}\alpha$ radiation with a voltage of 45 kV and a current of 40 mA was used with a step size of $0.01^\circ 2\theta$ and a count time of 40 s per step. Samples were scanned from 4° to $64^\circ 2\theta$. Following the XRD, the volcanic ashes were carbon coated and examined by scanning electron microscopy (SEM) with a Merlin Carl Zeiss SEM (CICT, Universidad de Jaén, Jaén, Spain).

Morphological analysis was done using secondary electron imaging (SE) and energy-dispersive X-ray (EDX) analysis to obtain textural and chemical data.

2.2. Zeta Potential

To study the electrical properties of the particles, the technique of electrophoretic mobility was used. This method requires working with particles of the order of micrometers, which has required the use of the finest fraction of the samples obtained by sieving.

For the electrical surface properties of the volcanic material, we have used the zeta potential, a parameter determined by the particle surface charge. To obtain the zeta potential, a small quantity of sample (0.05 g) was immersed in 20 mL of solutions of different electrolytes and concentration. The pH was adjusted between 2 and 10 using NaOH and HCl additions. Upon fitting with the pH measurements, we obtained electrophoretic mobility at $20.0 \pm 0.5^\circ\text{C}$ in a Malvern Zetasizer 3000 HS; the zeta potential was calculated based on the Smoluchowski approximation [33].

2.3. Surface Free Energy

To obtain the surface free energy components, the thin layer Wicking technique was used, for which the same fraction obtained by sieving was used. This method is based on measurement of the time t that a liquid of viscosity η and surface tension γ takes to penetrate a distance x through a thin, porous wall of a volcanic ash sample. The description of the process is given by a generalized form of equation of Washburn [7,21,34,35,39].

3. Results and Discussion

3.1. Compositional and Textural Characterization

The geochemical composition of the volcanic products of Tajogaite eruption correspond to basanite–tephrite with a content of SiO_2 ranging between 41% and 47% and total alkalis between 4% and 8% [40–42]. Lavas show a decrease of the alkalis, particularly in the first 20 days, from 6.4% to 4.6%, which is balanced by an analogous increase in MgO [41]. Our data (Table 1) agree with this evolution. Sample Jable-A, obtained one week after the start of the eruption, has 5.9% $\text{Na}_2\text{O} + \text{K}_2\text{O}$ and 6.7% MgO, while in sample Jable, at the end of the eruption, alkalis decrease to 4.7% and MgO increases to 8.8%. Also, the unaltered samples show high aluminum, iron, and calcium contents (13–15% Al_2O_3 ; 13% Fe_2O_3 ; 11% CaO), and a negligible volatile content. Nevertheless, it should be noted that the samples collected in areas with fumarolic activity differ significantly in the major elements, with the introduction of sulfur and a proportional decrease of other elements (Table 1).

Table 1. Major element composition (wt.% XRF) of ash samples.

% Oxides	SiO_2	Al_2O_3	Fe_2O_3	MnO	MgO	CaO	Na_2O	K_2O	TiO_2	P_2O_5	SO_4	Cl^-	Total
Jable-A	43.9	14.7	13.0	0.2	6.7	10.6	4.1	1.8	3.8	0.9	0.0	0.0	99.64
Jable	43.6	13.2	13.2	0.2	8.8	11.6	3.3	1.4	3.6	0.7	0.0	0.0	99.67
FUMA-1	47.1	10.7	9.9	0.1	6.6	9.8	2.5	1.0	3.6	0.8	5.2	1.1	98.46
FUMA-2	41.2	12.1	12.3	0.2	8.1	11.6	2.9	1.3	3.3	0.7	3.7	0.5	97.65

Mineralogically, the fresh ash samples studied are generally composed of clinopyroxenes, plagioclase, forsteritic olivine, and Fe oxides immersed in a glassy matrix with vesicular texture (Figure 2a,b). X-ray diffractograms show a high background, probably motivated by the presence of this amorphous vitreous material. Vesicles are very abundant, with rounded shape and a diameter of no more than several dozen of μm , except for some cases that reach around $100\ \mu\text{m}$ (Figure 2a). Zeolites are present only in some ashes. Specifically, those ashes affected by the fumarolic activity have as well as the native S and salts (halite, gypsum, hexahydrate, jarosite) and some Fe oxyhydroxides (Figure 2c).

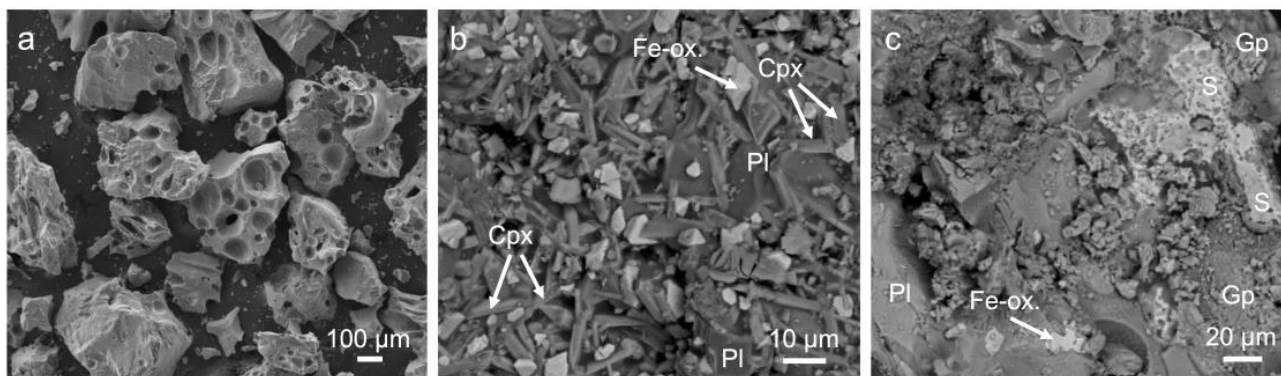


Figure 2. Secondary electron images of the studied ashes: (a) ash particles with a predominant diameter $< 0.5\ \text{mm}$ and with abundant vesicles; (b) detail of a fresh ash fragment with well-developed microphenocrysts of pyroxene (Cpx), plagioclase (Pl), and Fe-Ti oxides (Fe-ox.); (c) detail of an ash affected by the fumarolic activity with salts in its surface (gypsum, Gp) and an S coat.

3.2. Zeta Potential

In a first stage of the investigation, superficial ash collected one week after the start of the eruption (Jable-A) were compared with others collected three months after its end (Jable). The values of zeta potential for these two samples are negative for all pH values and positively correlated with its value, these being between -5 and $-50\ \text{mV}$ (Figure 3). This behavior is probably due to adsorption of H^+ and OH^- in the diffuse electric double layer; similar results appear in the bibliography [6,8,43,44]. It is also observed that the zeta potential values obtained for the Jable sample (after the eruption ended) are higher in absolute value than those corresponding to the first phases of the eruption, with differences of up to $10\ \text{mV}$ for some pHs.

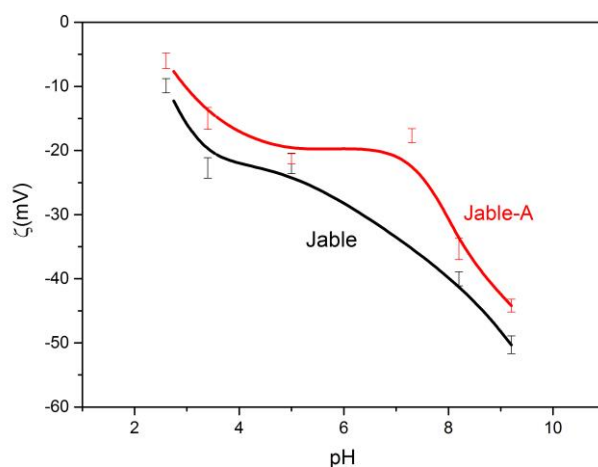


Figure 3. Zeta potential data of ash samples, one week after the start of the eruption (Jable-A red line) and three months after its end (Jable black line), for $0.1\ \text{mM}$ of NaCl as a function of the pH.

This gain in electrical charge that occurs over time is probably due to the different chemical nature of the expelled lava, since the first materials emitted by the volcano drag materials from the crust and the last ones correspond to a more basaltic material [40]. To avoid this variability in the value of the zeta potential over time, contemporary surface samples collected after the end of the eruption were studied, allowing us to compare the samples from the emission center with those located on the periphery.

With respect to the effect that the ionic strength of the medium has on the zeta potential values, it is noted that the ash has a negative surface electric charge and that this increases when the pH increases, as a general behavior in our samples (Figure 4). As expected, the zeta potential decreases with increasing ionic strength of the medium, due probably to double layer compression phenomena [7,45]. Also, it can be observed that the sample has an isoelectric point (IEP) at pH around 2. In the absence of ionic strength, the behavior of the graph is justified by the variation experienced by the ionic strength due to the variations in concentrations of H^+ and OH^- .

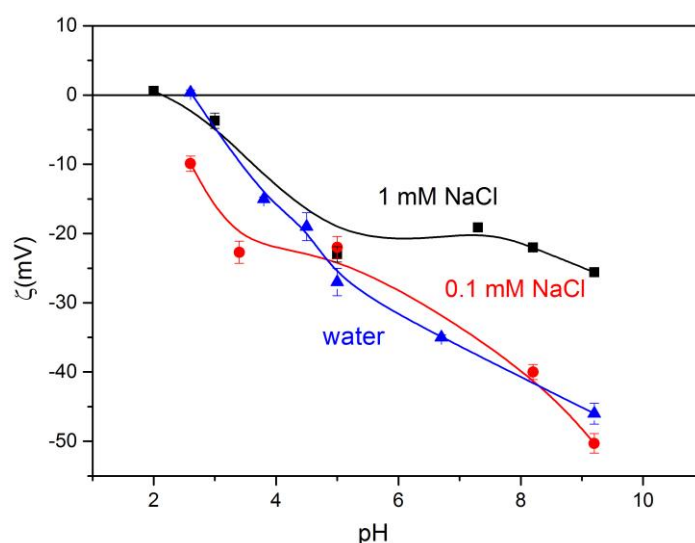


Figure 4. Zeta potential of ash sample Jable as a function of the pH for different ionic strengths.

In relation to the samples from the interior of the emission zone (FUMA 1 and 2) compared with those from the area around the volcano (Jable sample), the former presents a charge inversion with positive values for pH lower than 7.5 (IEP) (Figure 5). It can also be seen that the precipitate of sulfides and chlorides (FUMA 2) has a charge slightly higher than that of sulfur (FUMA 1) in absolute value, probably due to the presence of Al^{3+} and Fe^{3+} ions that give the material a positive charge at pH acids [8]. However, the general trend and the isoelectric point are the same and well differentiated with respect to the samples from the volcanic environment.

It can be seen that for FUMA 1 (inside the emission zone) the zeta potential reverses to positive and the zeta value of the ionic strength has no influence on the surface charge for pHs below the IEP, while for ashes outside the emission zone (Jable) they are clearly appreciable (Figure 6).

In the volcanic environment, the contribution of chemical species is common due to fumarolic activity; in addition, the ash is subjected to a continuous weathering process where the contribution of cations is significant. As a consequence, we have studied the effect on the surface charge of the ash of the more abundant mono-, di-, and tri-valent cations in the medium. The presence of these counter-ions demonstrates that volcanic ash particles undergo a charge neutralization at the IEP and then a charge reversal at high valence. Thus, a new electric double layer, where the mono-, di-, and tri-valent ions represent the counter-ion, is formed. With higher counter-ion valence, the charge neutralization occurs at higher pH values and the charge reversal is pronounced. These trends can be explained

by the larger screening effect of high-valence ions and the larger adsorption capability of high-valence counter-ions to the surface [23,45,46].

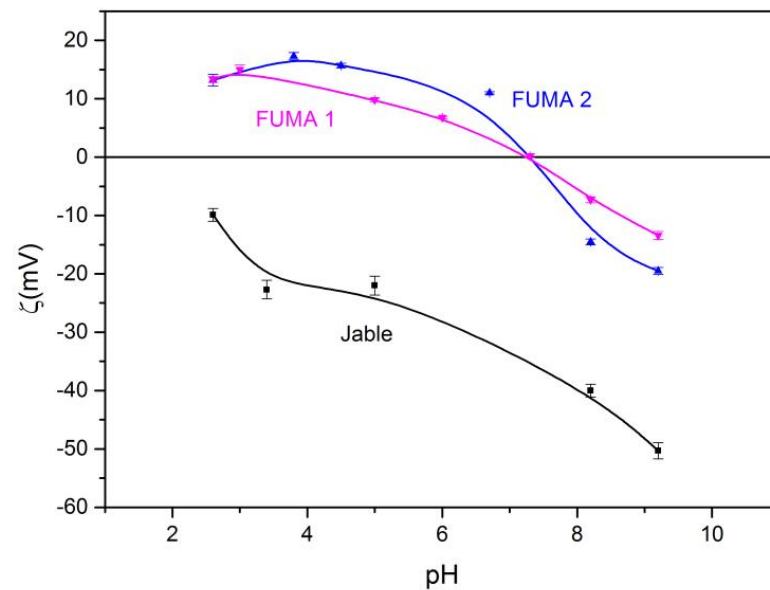


Figure 5. Zeta potential of volcanic ash samples as a function of the pH for 0.1 mM of NaCl for the different study places Jable, FUMA 1 and FUMA 2.

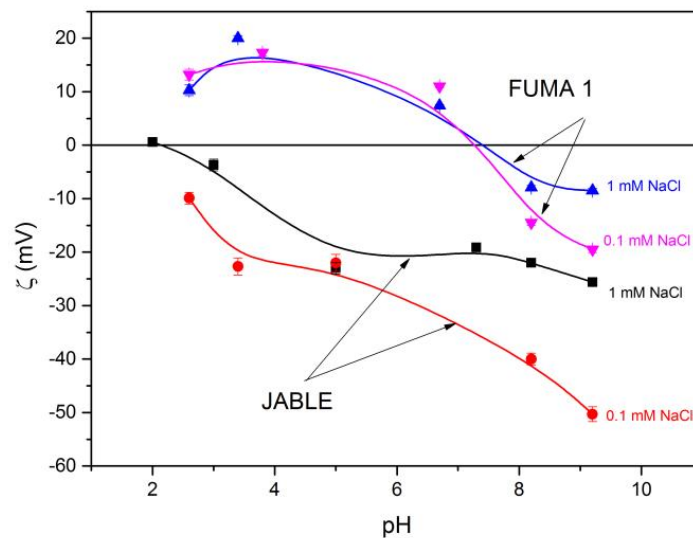


Figure 6. Zeta potential of volcanic ash samples as a function of the pH for 0.1 and 1 mM of NaCl for Jable and fumarolic places.

The zeta potential values of volcanic ash (FUMA 1 and Jable) treated with NaCl (monovalent), CaCl₂ (divalent), and FeCl₃ (trivalent) are shown in Figure 7. For the ash from the volcano environment (Jable sample), the zeta potential values in the case of mono- and di-valent ions are negative for the entire pH range (Figure 7a). Appreciable differences between these two ions are only seen at basic pH. For the iron ion, the values obtained are positive for pH less than 7, observing a charge inversion with an isoelectric point around pH = 6.3. At higher pH, negative but small zeta potential values are observed, of less than 10 mV.

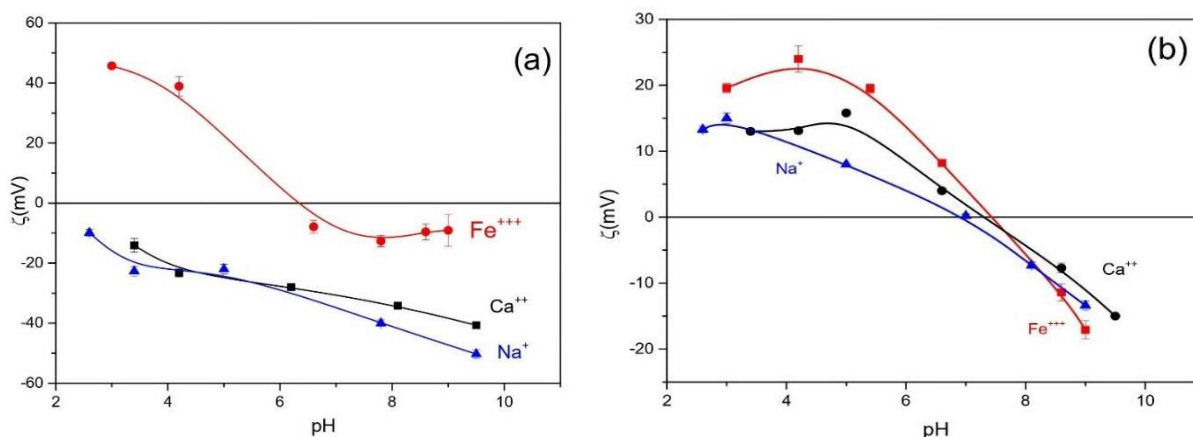


Figure 7. Zeta potential of volcanic ash samples as a function of the pH for 0.1 mM of NaCl, CaCl₂, and FeCl₃. (a) Jable; (b) FUMA 1.

As we analyze the effect of the different cations studied in the samples from inside the crater (FUMA 1 and 2) (Figure 7b), it can be seen that in all cases there is an IEP for pH values between 7 and 7.5. These samples have lower zeta potential values than those outside (Figure 7a), so the surface charge conferred to the particles is also lower.

As has been shown in the previous results, the surface properties are very sensitive to the contribution of different electrolytes in the medium. It is to be expected that over time there will be a contribution of organic matter to the deposit. For this reason, the effect of humic acids on the surface properties of the sampled deposits has been studied (Figure 8). It can be seen that at pH greater than 3 there is a significant charge increase of up to 15 mV when humic acids (HA) are present in the medium.

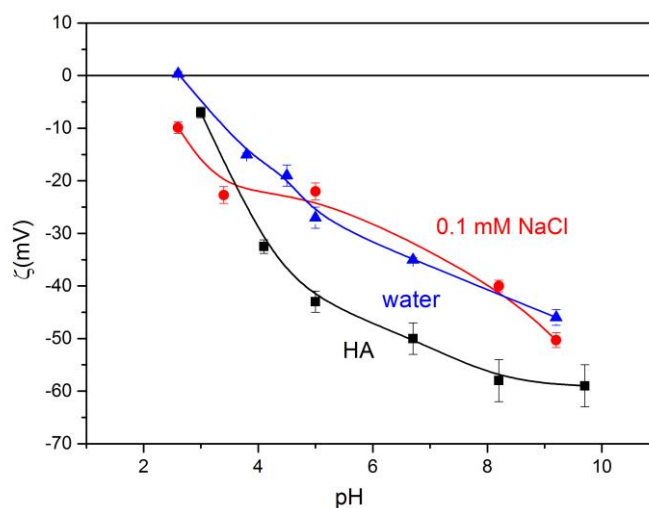


Figure 8. Comparative zeta potential values for Jable sample without ionic strength and treated with 0.1 mM of NaCl and 0.5 g/L of humic acid.

The zeta potential increased its negative charge at pH greater than 7, probably because of the ionization of HA molecules at basic pH. It is expected that the carboxyl groups are dissociated and negatively charged [47,48].

3.3. Surface Free Energy

The values of the surface free energy components, the total surface free energy, and the surface free energy LW and AB (ΔG^{LW} , ΔG^{AB}) of the ash samples obtained from the last eruption of the “Cumbre Vieja” volcano on the island of La Palma are shown in Table 2.

The total surface energy is obtained as the sum of the dispersive component (γ^{LW}) and the acid–base component, which is the geometric mean of the parameters γ^+ and γ^- .

Table 2. Surface free energy components, total surface free energy, and Gibbs free energy LW and AB for ash samples of eruption of “Cumbre Vieja” 2021.

Samples	γ^{LW} (mJ/m ²)	γ^- (mJ/m ²)	γ^+ (mJ/m ²)	γ^{Total} (mJ/m ²)	ΔG^{LW} (mJ/m ²)	ΔG^{AB} (mJ/m ²)
Jable-A	34 ± 3	75 ± 4	0.6 ± 0.7	48 ± 1	−2.8 ± 0.1	61.5 ± 1.2
Jable	55 ± 2	90 ± 3	0.15 ± 0.2	64 ± 5	−15.2 ± 1.1	115 ± 6
FUMA 1	61 ± 2	48 ± 4	0.15 ± 0.2	66 ± 9	−19.6 ± 1.0	35 ± 2
FUMA 2	41 ± 2	21 ± 2	6.7 ± 1.2	65 ± 4	−7.1 ± 1.2	−12.4 ± 0.8

In general, the ash has a monopolar nature ($\gamma^+ \approx 0$ and $\gamma^- \neq 0$), with electron-donor character, and these aspects do not change with the different treatments studied (Table 3). We highlight that the electron-donor component takes very high values, higher than 100 mJ/m², in some cases, conferring a strong hydrophilic character to the deposit and, therefore, a great water retention capacity.

Table 3. Surface free energy components, total surface free energy and Gibbs free energy LW and AB for ash samples of eruption of Tajogaite 2021, treated and non-treated with solutions Na, Ca, Fe and HA.

Samples		γ^{LW} (mJ/m ²)	γ^- (mJ/m ²)	γ^+ (mJ/m ²)	γ^{TOT} (mJ/m ²)	ΔG^{LW} (mJ/m ²)	ΔG^{AB} (mJ/m ²)	ΔG_{IF}^{TOT} (mJ/m ²)
Jable		55 ± 2	90 ± 3	0.15 ± 0.2	64 ± 5	−15.2 ± 1.1	115 ± 6	100 ± 7
	Na	50 ± 4	105 ± 13	1.8 ± 0.3	78 ± 3	−12 ± 2	77 ± 8	65 ± 9
	Ca	49 ± 5	45.6 ± 1.5	1.8 ± 0.1	67 ± 5	−11 ± 2	25 ± 5	14 ± 7
	Fe	49 ± 5	125 ± 10	0.65 ± 0.1	66 ± 6	−11 ± 2	104 ± 7	93 ± 9
	HA	58 ± 1	33 ± 2	6.9 ± 1.2	89 ± 4	−17.7 ± 0.5	7.0 ± 0.8	−10.7 ± 1.3
FUMA 1		61 ± 2	48 ± 4	0.15 ± 0.2	66 ± 9	−19.6 ± 1.0	35 ± 2	15 ± 3
	Na	61 ± 3	118 ± 11	4.1 ± 0.5	105 ± 9	−20 ± 2	70 ± 1	50 ± 3
	Ca	42.7 ± 2	87 ± 12	0.1 ± 0.1	48 ± 3	−7.1 ± 0.5	81 ± 5	74 ± 6
	Fe	61 ± 3	117 ± 10	0.2 ± 0.1	69 ± 7	−20 ± 3	108 ± 6	88 ± 9
FUMA 2		41 ± 2	21 ± 2	6.7 ± 1.2	65 ± 4	−7.1 ± 1.2	−12.4 ± 0.8	−20 ± 2
	Na	40 ± 1	36 ± 0.6	0.5 ± 0.1	48 ± 1	−5.3 ± 0.1	16.5 ± 0.5	11.2 ± 0.6
	Ca	59 ± 1	70 ± 3	40 ± 3	165 ± 8	−18 ± 1	−17 ± 3	−35 ± 4
	Fe	48 ± 1	67 ± 6	2 ± 0.5	68 ± 5	−10.2 ± 0.5	46 ± 4	36 ± 5

Table 2 also shows the sum total interaction energy of LW and acid–base interactions at a fixed distance $H_0 = 1.58 \text{ \AA}$. From these results, it can be seen that the effect of fumarolic activity is significant in the boiler samples (FUMA 1 and 2) where sulfur is present, possibly due to the formation of sulfides with these cations. These samples show an electron-donor component (γ^-) less than 50% with respect to the Jable sample. This behavior indicates a decrease of the hydrophilic character (less water retention); even for the FUMA 2 it showed an inversion in the character, reverting to the hydrophobic.

Table 3 shows the effect that different electrolytes have in the components of the surface free energy of volcanic materials, in particular, the effects of mono- (Na^+), di- (Ca^{++}) and tri-valent (Fe^{+++}) cations, which are the most abundant cations in the material ejected in the eruption (Table 1). Also, it shows the effect that humic acid has in the Jable sample, where there is vegetation. We can see the great sensitivity that the components of the surface free energy have to the presence of different chemical species present, highlighting the effect that humic acids produce. In any case, all these variations will be reflected in the interfacial component (LW + AB) of the total interaction energy between the ash particles.

3.4. Interaction Total Energy between Ash Particles

We calculate from the previous data (Zeta potential and surface free energy) the interaction energies between the sampled ash particles. The total interaction energy is calculated as the sum of two terms: the electrostatic and the thermodynamic. In the context of the van Oss model, the thermodynamic contemplates two contributions, a dispersive type (LW) interaction and an acid–base interaction in the Lewis sense [6,32]. The results of these energies will be presented as a function of the separation distance between the ash particles, using a spherical geometrical approximation [8]. Knowledge of these interaction energies will allow us to analyze the cohesion of a deposit, as well as its rheological properties in the case of sliding. The theoretical description of this method can be found in [32].

As expected between equal particles, the electrostatic component (ΔG^{EL}) is always repulsive, the greater the charge of the particles. On the contrary, the Lifshitz–van der Waals (ΔG^{LW}) interaction between peer entities is always attractive (Figure 9). And the acid–base component (ΔG^{AB}) at short distances is repulsive, although it can take negative values at longer distances depending on the nature of the acid–base interactions, which can include hydrogen bonding, structural interactions, hydrophobic attractions, or hydrophilic repulsions. The total interaction energy is also shown as the sum of the previous three (Figure 9).

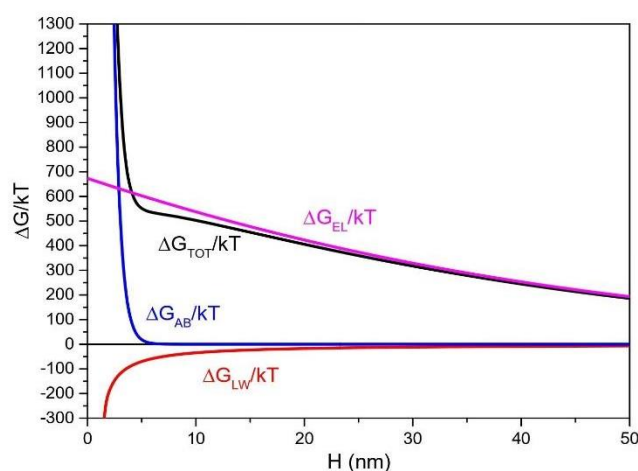


Figure 9. Total interaction energy and its components as a function of the distance between two ash particles (Jable sample) at pH = 6 and ionic strength 0.1 mM of NaCl.

The effect of the ionic force on the repulsions between particles is clearly observed, these being greater at a lower ionic force (Figure 10). On the other hand, it is significant to observe the potential well that occurs for acidic pH (Figure 10a) and at the highest ionic strength studied. This behavior is justified because the electrical component is almost null and the dispersive component LW (attractive) at these distances is the predominant one.

From the results presented in Figure 11a, it can be deduced that the cohesion inside the crater (FUMA 1) is greater than the others, presenting a potential well between 50 and 170 kT depending on the pH. This well is less at acid pHs. Potential barriers are observed for the ash furthest away from the source of emission, unaffected by fumarolic activity. Figure 11b shows the total interaction energy of the three samples studied at pH = 7.2, which is the isoelectric point of the crater samples. In this situation, the zeta potential is zero, so the electrical component of the total energy is zero. Therefore, the differences in the results are only justified by the different values of the dispersive and acid–base components. Based on this, it can be affirmed that in the case of the precipitates of FUMA 1, due to the fumarolic activity in the crater, they confer greater stability to the deposit than in the distal samples.

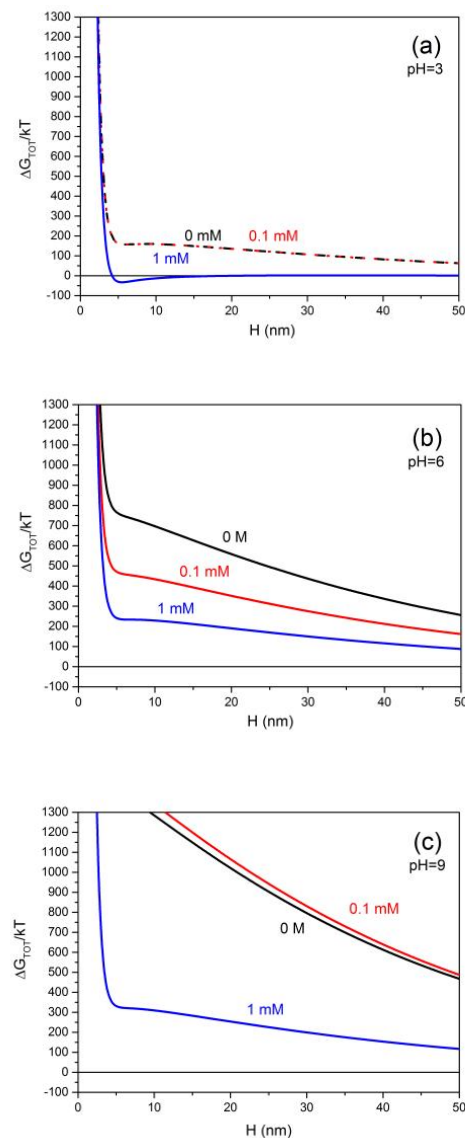


Figure 10. Total interaction energy for different ionic strengths of NaCl (0, 1 and 0.1 mM) for (a) acidic pH (3), (b) natural pH (6) and (c) basic pH (9), as a function of the separation distance between particles, for Jable sample.

With respect to the interaction energies between ash particles when they are in different ionic media (Na^+ , Ca^{++} and Fe^{+++}) for the samples from Jable point view (Figure 12a) and FUMA 1 (Figure 12b), in all cases there is a potential barrier except in the presence of Fe at pH close to the isoelectric point, where there is a net attraction. In any case, if we consider that below 200 kT the deposit is stable, it can be seen that there will be high instability with Na and Ca cations for pH higher than 6; while with Fe it is only observed at acidic pHs due to the excess of positive charge that the ash acquires in the presence of Fe at these pHs (Figure 12a).

Considering the interaction energies between the ash particles, the apparently homogeneous tephra shows a marked heterogeneity, both by alteration due to fumarolic activity and by simple washing by rain, in the case of unaltered samples. Furthermore, all samples show a heterogeneous response to changes in the cation nature and concentration solution for pH from 2 to 10. This variability implies that the tephra cohesion of a single eruption event will also be heterogeneous, with abrupt decreases that can jeopardize the stability of the deposit, e. g. when Fe is liberated in an acid environment, as can occur in an acid rain event, common in some eruptions.

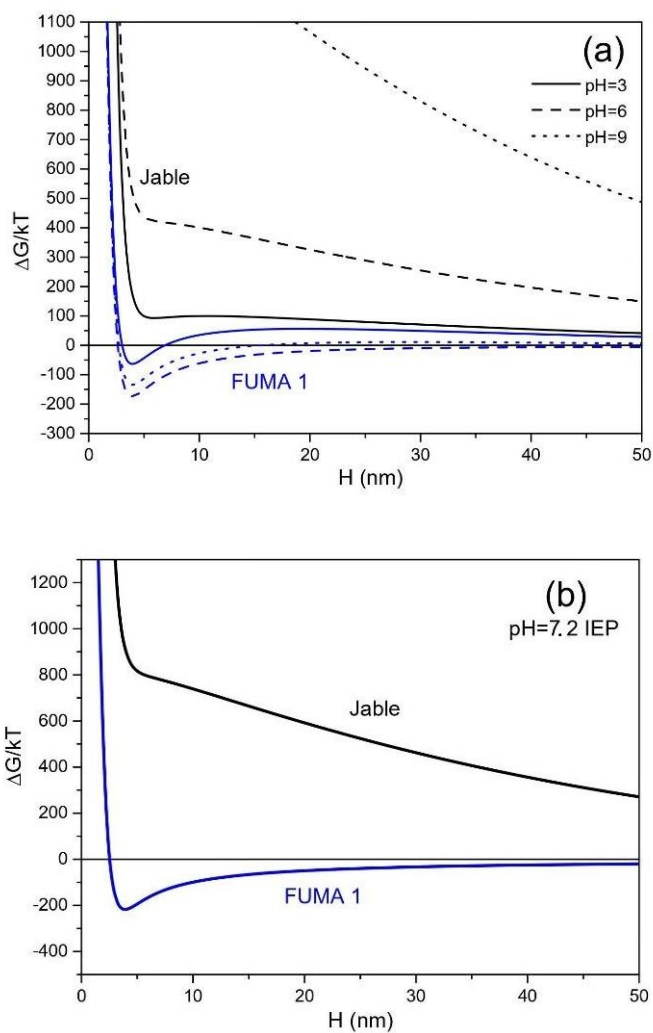


Figure 11. Total interaction energy at 0.1 mM of NaCl at: (a) different pHs (solid line pH = 3, dash pH = 6, dot pH = 9); (b) at pH= 7.2 (IEP). For Jable and FUMA 1 samples.

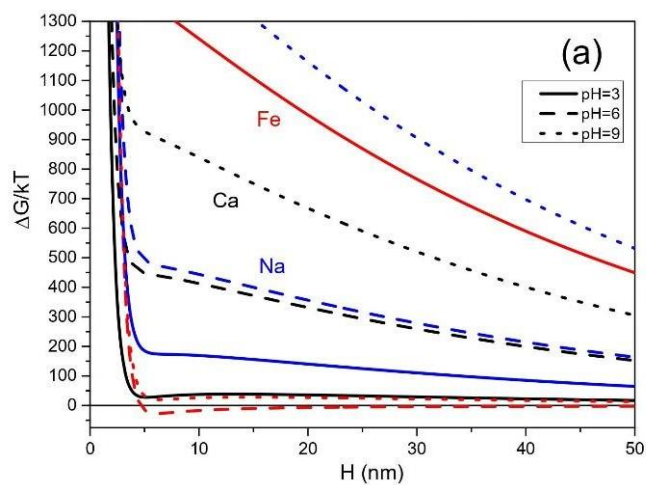


Figure 12. Cont.

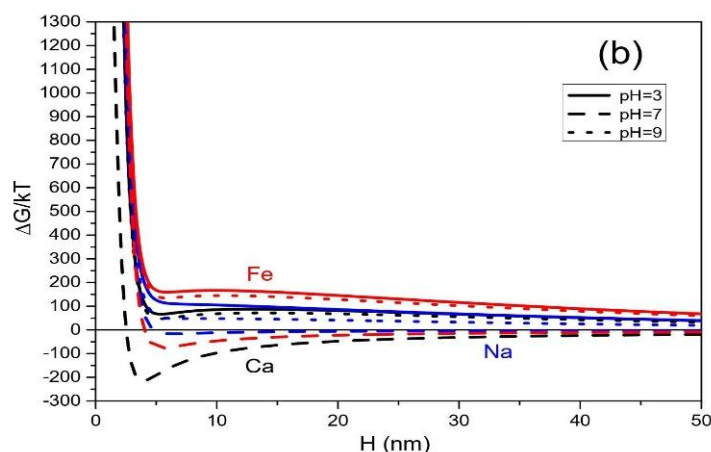


Figure 12. Total interaction energy for different pHs (solid line pH = 3, dash pH = 6, dot pH = 9) for (a) Jable sample and (b) FUMA 1 sample with ionic strength 0.1 mM of different ionic media (Na, Ca and Fe).

4. Conclusions

The deposits of the 2021 Tajogaite eruption from Cumbre Vieja volcano are relatively uniform in the basanite–tephrite field, but fumarolic activity altered their composition early on with native S, salts (halite, gypsum, hexahydrate, jarosite), and some Fe oxyhydroxide. The morphological analysis indicates that in general it is a much vesiculated material, and that zeolites are present only in some ashes.

The zeta potential values of volcanic ash are negative, increase with increasing pH, and decrease when the ionic strength of the medium increases. With fumarolic activity, either sulfur and sulphate dominated, over the tephra deposits reverses the sign of the zeta potential for acidic pH, and in this pH range the zeta potential is indifferent to the ionic strength. The addition of different cations produces significant changes in the zeta potential. Their values increase with the valence for acidic pH values; on the other hand, for basic pH values they decrease. In the fumarolically altered samples, the charge generated at the surface is considerably less. The addition of humic acids increases, in all the cases studied, the zeta potential values of volcanic ash.

Regarding the surface free energy data, it can be deduced that fumarolically altered samples have a reduction close to 50% in the electron-donor component compared to the unaltered samples. This behavior indicates a decrease in hydrophilic character, that is, less water retention. Even in one of the altered samples (FUMA 2), its characteristics are reversed and it becomes hydrophobic.

With respect to the total interaction energy between ash particles, ash deposits are generally more cohesive with lower pH and have higher ionic strength. Fumarolically altered samples have potential wells (attractive interaction), which implies even greater stability. Among the cations that can modify the interaction energies, the effect of Fe stands out, which at acidic pH presents a large potential barrier that is not observed in the other cations. In this situation, there would be little cohesion.

In short, our research shows that a single volcanic event with a near homogeneous geochemical deposit can present heterogeneous distribution of particle interaction values in a brief period after the eruption. These differences are due to an early weathering (rain washing) or fumarolic alteration, which acts in the sense of destabilizing or stabilizing respectively the ash deposits. On the other hand, the reduction of hydrophilicity in the tephra affected by fumaroles will reduce the weight of the deposit in the rainy season, also favoring its mechanical stability. Subsequent alterations in the environment due to the contribution of metals could modify the interaction energies and therefore the cohesion, which in the case of the iron at acid pH can strongly reduce the stability of the ash deposit. Although there are other factors that influence the stability of the volcanic slope (e.g., particle size and geometry), the factors described in this work are also decisive. Therefore,

a heterogeneous geomechanical behavior of the volcanic building is expected, with a rapid and reactive evolution in the face of environmental changes, which should be taken into account for stability studies.

Author Contributions: Conceptualization, A.O.-O. and J.A.M.-B.; methodology, A.O.-O. and J.A.M.-B.; validation, A.O.-O., J.A.M.-B., R.H.M., I.A. and M.S.-G.; formal analysis, A.O.-O., J.A.M.-B., R.H.M., I.A. and M.S.-G.; investigation, A.O.-O., J.A.M.-B., R.H.M., I.A. and M.S.-G.; writing—original draft preparation, A.O.-O. and J.A.M.-B.; writing—review and editing, A.O.-O., J.A.M.-B., I.A. and M.S.-G.; supervision, A.O.-O., J.A.M.-B., I.A. and M.S.-G.; project administration, A.O.-O. and J.A.M.-B. All authors have read and agreed to the published version of the manuscript.

Funding: This work has been funded by project SUPRODEI (PID2022-139813NB-I00) financed by (MCIN/AEI/10.13039/501100011033/FEDER, EU) of the Spanish Ministry of Science and Innovation.

Data Availability Statement: Data are contained within the article.

Acknowledgments: This is a short text to acknowledge the contributions of specific colleagues, institutions, or agencies that aided the efforts of the authors. Technical and human support provided by Centro de Instrumentación Científico-Técnica (CICT)-Servicios Centrales de Apoyo a la Investigación (SCAI)-Universidad de Jaén (UJA, Junta de Andalucía, FEDER), is gratefully acknowledged.

Conflicts of Interest: The authors declare no conflict of interest.

References

1. Sinarta, N.I.; Rifa'i, A.; Fathani, T.F.; Wilopo, W. Geotechnical properties and geology age on characteristics of landslides hazards of volcanic soils in Bali, Indonesia. *Int. J. Geomate* **2016**, *11*, 2595–2599.
2. IGN., 2021, Report. Available online: <https://www.ign.es/web/recursos/volcanologia/> (accessed on 1 May 2023).
3. IGME-CSIC., 2021, Report, “Operación Cenicienta”. Available online: <https://info.igme.es/eventos/Erupcion-volcanica-la-palma/> (accessed on 1 May 2023).
4. Bonadonna, C.; Pistolesi, M.; Biass, S.; Voloschina, M.; Romero, J.; Coppola, D.; Folch, A.; D’auria, L.; Martin-Lorenzo, A.; Dominguez, L.; et al. Physical Characterization of Long-Lasting Hybrid Eruptions: The 2021 Tajogaite Eruption of Cumbre Vieja (La Palma, Canary Islands). *J. Geophys. Res. Solid Earth* **2022**, *127*, e2022JB025302. [[CrossRef](#)]
5. Bonadonna, C.; Pistolesi, M.; Dominguez, L.; Freret-Lorgeril, V.; Rossi, E.; Fries, A.; Biass, S.; Voloschina, M.; Lemus, J.; Romero, J.E.; et al. Tephra sedimentation and grainsize associated with pulsatory activity: The 2021 Tajogaite eruption of Cumbre Vieja (La Palma, Canary Islands, Spain). *Front. Earth Sci.* **2023**, *11*, 1166073. [[CrossRef](#)]
6. Ontiveros-Ortega, A.; Moleón, J.A.; Plaza, I.; Guillén, C. Effect of interfacial properties on mechanical stability of ash deposit. *J. Rock Mech. Geotech. Eng.* **2016**, *8*, 187–197. [[CrossRef](#)]
7. Ontiveros-Ortega, A.; Plaza, I.; Calero, J.; Moleón, J.A.; Ibañez, J.M. High variability of interaction energy between volcanic particles: Implications for deposit stability. *Nat. Hazards* **2023**, *117*, 3103–3122. [[CrossRef](#)]
8. Plaza, I.; Ontiveros-Ortega, A.; Calero, J.; Romero, C. A new approach to triggering mechanism of volcano landslides based on zeta potential and surface free energy balance. *Geomorphology* **2018**, *301*, 1–9. [[CrossRef](#)]
9. Li, Z.; Giese, R.F.; Wu, W.; Sheridan, M.F.; van Oss, C.J. The Surface Thermodynamic Properties of Some Volcanic Ash Colloids. *J. Dispers. Sci. Technol.* **1997**, *18*, 223–241. [[CrossRef](#)]
10. Bailey, C.; Fodor-Csorba, K.; Gleeson, J.T.; Sprunt, S.N.; Jáklí, A. Rheological properties of bent-core liquid crystals. *Soft Matter* **2009**, *5*, 3618–3622. [[CrossRef](#)]
11. Cockell, C.S. Geomicrobiology beyond Earth: Microbe–mineral interactions in space exploration and settlement. *Trends Microbiol.* **2010**, *18*, 308–314. [[CrossRef](#)]
12. Gimmi, T.; Kosakowski, G. How Mobile Are Sorbed Cations in Clays and Clay Rocks? *Environ. Sci. Technol.* **2011**, *45*, 1443–1449. [[CrossRef](#)]
13. Baumgarten, W.; Neugebauer, T.; Fuchs, E.; Horn, R. Structural stability of marshland soils of the riparian zone of the tidal Elbe River. *Soil Tillage Res.* **2012**, *125*, 80–88. [[CrossRef](#)]
14. Baumgarten, W.; Dörner, J.; Horn, R. Microstructural development in volcanic ash soils from South Chile. *Soil Tillage Res.* **2013**, *129*, 48–60. [[CrossRef](#)]
15. Kadar, E.; Fisher, A.; Stolpe, B.; Calabrese, S.; Lead, J.; Valsami-Jones, E.; Shi, Z. Colloidal stability of nanoparticles derived from simulated cloud-processed mineral dusts. *Sci. Total. Environ.* **2014**, *466–467*, 864–870. [[CrossRef](#)]
16. Chester, F.M.; Rowe, C.; Ujiie, K.; Kirkpatrick, J.; Regalla, C.; Remitti, F.; Moore, J.C.; Toy, V.; Wolfson-Schwehr, M.; Bose, S.; et al. Structure and Composition of the Plate-Boundary Slip Zone for the 2011 Tohoku-Oki Earthquake. *Science* **2013**, *342*, 1208–1211. [[CrossRef](#)] [[PubMed](#)]

17. Kameda, J.; Inaoi, C.; Conin, M. Exchangeable cation composition of the smectite-rich plate boundary fault at the Japan Trench. *Geophys. Res. Lett.* **2016**, *43*, 3112–3119. [[CrossRef](#)]
18. Kameda, J.; Morisaki, T. Sensitivity of Clay Suspension Rheological Properties to pH, Temperature, Salinity, and Smectite-Quartz Ratio. *Geophys. Res. Lett.* **2017**, *44*, 9615–9621. [[CrossRef](#)]
19. Kameda, J.; Uno, M.; Conin, M.; Ujiie, K.; Hamada, Y.; Kimura, G. Fault weakening caused by smectite swelling. *Earth, Planets Space* **2019**, *71*, 1–7. [[CrossRef](#)]
20. Kameda, J.; Hamada, Y. Cohesive slip at the subduction boundary of a plate during a large earthquake. *Geophys. Res. Lett.* **2020**, *47*, e2020GL088395. [[CrossRef](#)]
21. Ontiveros-Ortega, A.; Vidal, F.; Gimenez, E.; and Ibáñez, J.M. Effect of heavy metals on the surface free energy and zeta potential of volcanic glass: Implications on the adhesion and growth of microorganisms. *J. Mater. Sci.* **2014**, *49*, 3550–3559. [[CrossRef](#)]
22. Nakamoto, K.; Kamei, M.; Kameda, J. Surface Physicochemical Properties of Smectite-Rich Fault Gouge: A Case Study of the Japan Trench Plate-Boundary Fault. *Geophys. Res. Lett.* **2023**, *50*, e2023GL104271. [[CrossRef](#)]
23. Pavlovic, M.; Huber, R.; Adok-Sipiczki, M.; Nardin, C.; Szilagyi, I. Ion specific effects on the stability of layered double hydroxide colloids. *Soft Matter* **2016**, *12*, 4024–4033. [[CrossRef](#)] [[PubMed](#)]
24. Borgia, A.; Lanari, R.; Sansosti, E.; Tesauro, M.; Bernardino, P.; Fornaro, G.; Neri, M.; Murray, J.B. Actively growing anticlines beneath catania from the distal motion of Mount Etna's Decollement measured by SAR interferometry and GPS. *Geophys. Res. Lett.* **2000**, *27*, 3409–3412. [[CrossRef](#)]
25. Bonaccorso, A.; Currenti, G.; Del Negro, C. Interaction of volcano-tectonic fault with magma storage, intrusion and flank instability: A thirty years study at Mt. Etna volcano. *J. Volcanol. Geotherm. Res.* **2013**, *251*, 127–136. [[CrossRef](#)]
26. Murray, J.B.; van Wyk de Vries, B.; Pitty, A.; Sargent, P.; Wooller, L. Gravitational sliding of the Mt. Etna massif along a sloping basement. *Bull. Volcanol.* **2018**, *80*, 1–11. [[CrossRef](#)]
27. Wooller, L.; van Wyk de Vries, B.; Murray, J.B.; Rymer, H.; Meyer, S. Volcano spreading controlled by dipping substrata. *Geology* **2004**, *32*, 573–576. [[CrossRef](#)]
28. Amonte, C.; Melián, G.V.; Asensio-Ramos, M.; Pérez, N.M.; Padrón, E.; Hernández, P.A.; D'auria, L. Hydrogeochemical temporal variations related to the recent volcanic eruption at the Cumbre Vieja Volcano, La Palma, Canary Islands. *Front. Earth Sci.* **2022**, *10*, 1003890. [[CrossRef](#)]
29. Witham, C.S.; Oppenheimer, C.; Horwell, C.J. Volcanic ash-leachates: A review and recommendations for sampling methods. *J. Volcanol. Geotherm. Res.* **2005**, *141*, 299–326. [[CrossRef](#)]
30. Sun, S.-S.; Ao, M.; Geng, K.-R.; Chen, J.-Q.; Deng, T.-H.; Li, J.-J.; Guan, Z.-T.; Mo, B.-L.; Liu, T.; Yang, W.-J.; et al. Enrichment and speciation of chromium during basalt weathering: Insights from variably weathered profiles in the Leizhou Peninsula, South China. *Sci. Total. Environ.* **2022**, *822*, 153304. [[CrossRef](#)]
31. Dupla, X.; Möller, B.; Baveye, P.C.; Grand, S. Potential accumulation of toxic trace elements in soils during enhanced rock weathering. *Eur. J. Soil Sci.* **2023**, *74*, e13343. [[CrossRef](#)]
32. van Oss, C.J. Polar or Lewis acid-base interactions. In *Interfacial forces in Aqueous Media*; CRC Press: Boca Raton, FL, USA, 1994; pp. 18–46.
33. Smoluchowski, M.V. Electroosmosis. In *Handbuch der Elektrizität und des Magnetismus*; Barth: Leipzig, Germany, 1921; p. 366.
34. Washburn, E.W. The Dynamics of Capillary Flow. *Phys. Rev. B* **1921**, *17*, 273–283. [[CrossRef](#)]
35. Chibowski, E. Solid surface free energy components determination by the thin-layer wicking technique. *J. Adhes. Sci. Technol.* **1992**, *6*, 1069–1090. [[CrossRef](#)]
36. Chibowski, E.; Holysz, L. Use of the Washburn equation for surface free energy determination. *Langmuir* **1992**, *8*, 710–716. [[CrossRef](#)]
37. Campeny, M.; Menéndez, I.; Ibáñez-Insa, J.; Rivera-Martínez, J.; Yepes, J.; Álvarez-Pousa, S.; Méndez-Ramos, J.; Mangas, J. The ephemeral fumarolic mineralization of the 2021 Tajogaite volcanic eruption (La Palma, Canary Islands, Spain). *Sci. Rep.* **2023**, *13*, 1–14. [[CrossRef](#)]
38. Martínez-Martínez, J.; Mediato, J.F.; Mata, M.P.; Ordóñez, B.; del Moral, B.; Bellido, E.; Pérez-López, R.; Rodríguez-Pascua, M.A.; Vegas, J.; Lozano-Otero, G.; et al. Early fumarolic minerals from the Tajogaite volcanic eruption (La Palma, 2021). *J. Volcanol. Geotherm. Res.* **2023**, *435*, 107771. [[CrossRef](#)]
39. Duran, J.D.G.; Ontiveros, A.; Delgado, A.V.; Gonzalez-Caballero, F. Kinetics and interfacial interactions in the adhesion of colloidal calcium carbonate to glass in a packed-bed. *Appl. Surf. Sci.* **1998**, *134*, 125–138. [[CrossRef](#)]
40. Castro, J.M.; Feisel, Y. Eruption of ultralow-viscosity basanite magma at Cumbre Vieja, La Palma, Canary Islands. *Nat. Commun.* **2022**, *13*, 3174. [[CrossRef](#)] [[PubMed](#)]
41. Day, J.M.D.; Troll, V.R.; Aulinas, M.; Deegan, F.M.; Geiger, H.; Carracedo, J.C.; Pinto, G.G.; Perez-Torrado, F.J. Mantle source characteristics and magmatic processes during the 2021 La Palma eruption. *Earth Planet. Sci. Lett.* **2022**, *597*, 117793. [[CrossRef](#)]
42. Romero, J.E.; Burton, M.; Cáceres, F.; Taddeucci, J.; Civico, R.; Ricci, T.; Pankhurst, M.J.; Hernández, P.A.; Bonadonna, C.; Llewellyn, E.W.; et al. The initial phase of the 2021 Cumbre Vieja ridge eruption (Canary Islands): Products and dynamics controlling edifice growth and collapse. *J. Volcanol. Geotherm. Res.* **2022**, *431*, 107642. [[CrossRef](#)]
43. Aizawa, K. Classification of self-potential anomalies on volcanoes and possible interpretations for their subsurface structure. *J. Volcanol. Geotherm. Res.* **2008**, *175*, 253–268. [[CrossRef](#)]

44. Aizawa, K.; Uyeshima, M.; Nogami, K. Zeta potential estimation of volcanic rocks on 11 island arc-type volcanoes in Japan: Implication for the generation of local self-potential anomalies. *J. Geophys. Res. Atmos.* **2008**, *113*, B02201. [[CrossRef](#)]
45. Li, M.; Kobayashi, M. The aggregation and charging of natural clay allophane: Critical coagulation ionic strength in the presence of multivalent counter-ions. *Colloids Surfaces A Physicochem. Eng. Asp.* **2021**, *626*, 127021. [[CrossRef](#)]
46. Cao, T.; Elimelech, M. Colloidal stability of cellulose nanocrystals in aqueous solutions containing monovalent, divalent, and trivalent inorganic salts. *J. Colloid Interface Sci.* **2020**, *584*, 456–463. [[CrossRef](#)] [[PubMed](#)]
47. Ramos-Tejada, M.M.; Ontiveros, A.; Viota, J.L.; Durán, J.D.G. Interfacial and rheological properties of humic acid/hematite suspensions. *J. Colloid Interface Sci.* **2003**, *268*, 85–95. [[CrossRef](#)]
48. Plaza, I.; Ontiveros-Ortega, A.; Calero, J.; Aranda, V. Implication of zeta potential and surface free energy in the description of agricultural soil quality: Effect of different cations and humic acids on degraded soils. *Soil Tillage Res.* **2015**, *146*, 148–158. [[CrossRef](#)]

Disclaimer/Publisher's Note: The statements, opinions and data contained in all publications are solely those of the individual author(s) and contributor(s) and not of MDPI and/or the editor(s). MDPI and/or the editor(s) disclaim responsibility for any injury to people or property resulting from any ideas, methods, instructions or products referred to in the content.